THE LANDFALL AND STRUCTURE OF A TROPICAL CYCLONE: THE SENSITIVITY OF MODEL PREDICTIONS TO SOIL MOISTURE PARAMETERIZATIONS

ASHU DASTOOR and T. N. KRISHNAMURTI

Department of Meteorology, Florida State University, Tallahassee, FL 32306, U.S.A.

(Received in final form 20 December, 1990)

Abstract. A regional mesoscale multi-level primitive equation model is used to predict the landfall and structure of a tropical cyclone. Three areas of model sensitivity are addressed in this paper; (1) the horizontal resolution, which includes the representation of orography; (2) the impact of an improved representation of the distribution of land surface soil moisture on the landfall problem; and (3) the sensitivity of the storm to lateral boundary conditions. A diagnostic part of this study describes a statistical regression approach to determining a ground wetness parameterization from moisture budget computations to derive estimates of surface fluxes, which are used to determine the parameterization. The model sensitivity analysis compares several versions of ground wetness parameterization. The experiment where 'perfect' (i.e., based on analysis of observations) boundary conditions are used is defined as a bench-mark. At the highest horizontal resolution (=50 km) using the ground wetness obtained from the regression, the best results were found for the structure and motion of the tropical cyclone. When the boundary conditions from a global model are used at a resolution T106 (roughly 100 km resolution for the transformed grid), the results degrade somewhat. The rain bands are predicted, but do not contain the same detail. Several other sensitivity experiments illustrate the degree of degradation of rain bands, precipitation distribution, hurricane structure, and phase speed errors as the lateral boundaries, resolution, and ground wetness parameterization are altered.

1. Introduction

An essential factor in the estimation of surface evaporation is the parameterization of soil moisture. Many soil moisture sensitivity experiments (Walker and Rowntree, 1977; Yeh *et al.*, 1984; Sud and Fennessy, 1984; Sud and Smith, 1985; Kitoh *et al.*, 1988; Sud and Molod, 1988) have confirmed the importance of its parameterization in climate models. The general conclusion of these experiments is that reduced soil moisture causes a reduction in evaporation, which in turn decreases rainfall. Accurate initial conditions were shown to be important in the context of predictions on time scales from a few hours or days (Walker and Rowntree, 1977; Rowntree and Bolton, 1983) up to several months (Carson and Sangster, 1981).

Soil moisture/ground wetness is a difficult parameter to estimate since it depends on evaporation, rainfall, snowmelt, infiltration and surface runoff as well as vegetation. For a layer of ground between depths z and $z - \partial z$, neglecting horizontal sub-surface transfer of water, the generalized equation for soil moisture change can be written as

Boundary-Layer Meteorology **55**: 345–380, 1991.

$$\frac{\partial m_s(z)}{\partial t} = -\frac{\partial M(z)}{\partial z} + N(z) \tag{1.1}$$

where

$m_s(z)$ = soil moisture at depth z

$M(z)$ = moisture flux at depth z

$N(z)$ = source/sink term at depth z.

At the surface, moisture flux is given as

$$M(0) = -E(0) + (P + M_s - Y(0)) \tag{1.2}$$

where

$E(0)$ = evapotranspiration

P = precipitation rate

M_z = snowmelt

$Y(0)$ = surface runoff.

A ground wetness parameter can be defined as the fractional soil moisture at the surface:

$$GW = \frac{m_s(0)}{m_{s|\max}} \tag{1.3}$$

where $m_{s_{\max}}$ is the maximum value (field capacity) of $m_s(0)$.

To parameterize the above, many simplifications are made in the models. One of the widely used methods in climate models was first introduced by Manabe (1969a) resulting from Soviet observational studies by Romanova (1954), who found that for plains and forest regions, most of the moisture change takes place in the top one meter of soil, which usually encompasses the root zone of moist vegetation. Manabe's scheme uses a one-layer water budget equation which includes a simple parameterization for evaporation, precipitation, surface runoff and snowmelt. Field capacity is taken constant for all land points. The ground wetness sensitivity experiments, reviewed by Mintz (1984), use relatively simple parameterization schemes and lack geographical variations of most surface characteristics. More complex schemes have been developed in recent years which include the geographic variations of albedo, roughness length and root depth (Hansen *et al.*, 1983; Dickinson, 1984; Sellers *et al.*, 1986).

Most numerical regional models use a rather simple parameterization for ground wetness. The NCAR/Penn State University limited-area model, the JMA Tokyo regional spectral model and the ECMWF limited-area model use climatologically specified values for ground wetness (a list of acronyms and symbols is provided

TABLE I

List of acronyms

NCAR	National Center for Atmospheric Research
JMA	Japan Meteorological Agency
RH	Relative Humidity
GW	Ground Wetness
ECMWF	European Centre for Medium Range Weather Forecasting
FSU	Florida State University
SST	Sea Surface Temperature
FGGE	First GARP global experiment
GWM1	Ground wetness (first empirical relation)
GWM2	Ground wetness (second empirical relation)

in Table I). The French weather service limited-area model uses a one-layer predictive equation for soil moisture. In the FSU regional model (Krishnamurti *et al.*, 1990), the following two empirical relations for ground wetness were used:

$$GWM1 = \frac{(\alpha_{\max} - \alpha)}{(\alpha_{\max} - \alpha_{\min})}(1 - RH) \tag{1.4}$$

$$GWM2 = 0.85[1.0 - \exp\{-200.0(0.25 - \alpha)^2\}] \tag{1.5}$$

where α is surface albedo and RH is relative humidity for the layer nearest to the ground. Climatologically specified values of ground wetness given by empirical relations such as Equations (1.4) and (1.5) do not take account of changes in soil moisture due to past rainfall and other surface changes. If a predictive equation is used for GW (Ground Wetness) as in the French weather service model, one faces the problem of getting reliable initial values for ground wetness besides the difficulties of parameterizing the various fluxes involved.

In the present study, we propose a new scheme for parameterization of ground wetness. This procedure can be used to obtain initial values for ground wetness and thus to initialize the model. Further, it provides an expression for ground wetness which depends only on rainfall and other large-scale surface parameters.

2. FSU Regional Model

A description of the FSU high resolution regional model and its performance is found in Krishnamurti *et al.* (1990). Details will not be presented here, but a list of pertinent references is given in Krishnamurti *et al.* (1990). Figure 1 illustrates the three different grids used, viz., the 1.875°, 0.938° and 0.469° latitude/longitude meshes. Figure 2 illustrates some of the other relevant basic data fields, including (a) the sea surface temperature °K, (b) the surface albedo and (c) the terrain heights (m) for the highest resolution. The domains for the 1.875°, 0.938°, and 0.469° meshes are respectively bounded by (30 E to 150 E, 30 S to 40 N), (45 E to 118 E, 8 S to 41 N), and (51.6 E to 107.3 E, 8.9 S to 38.9 N).

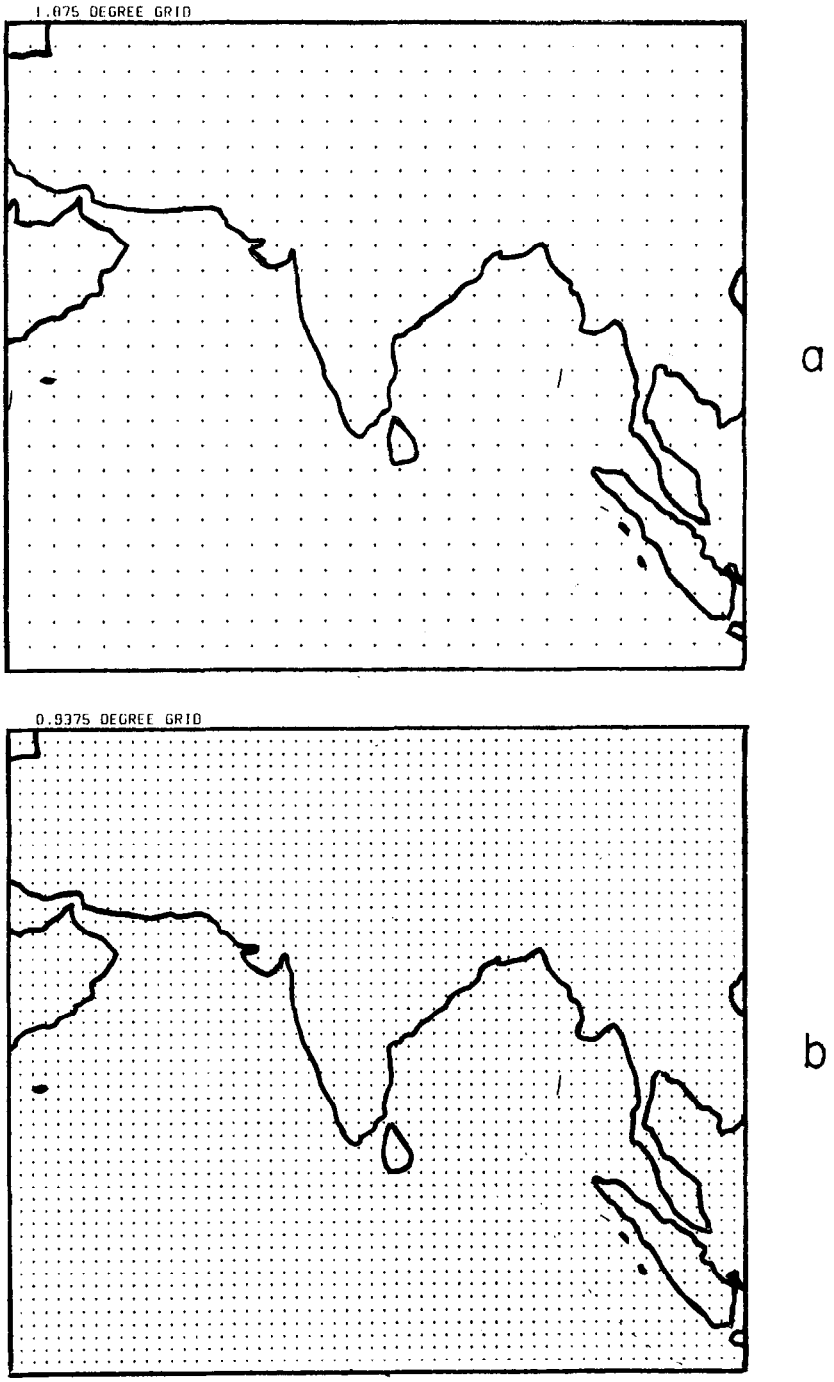

Fig. 1a, b.

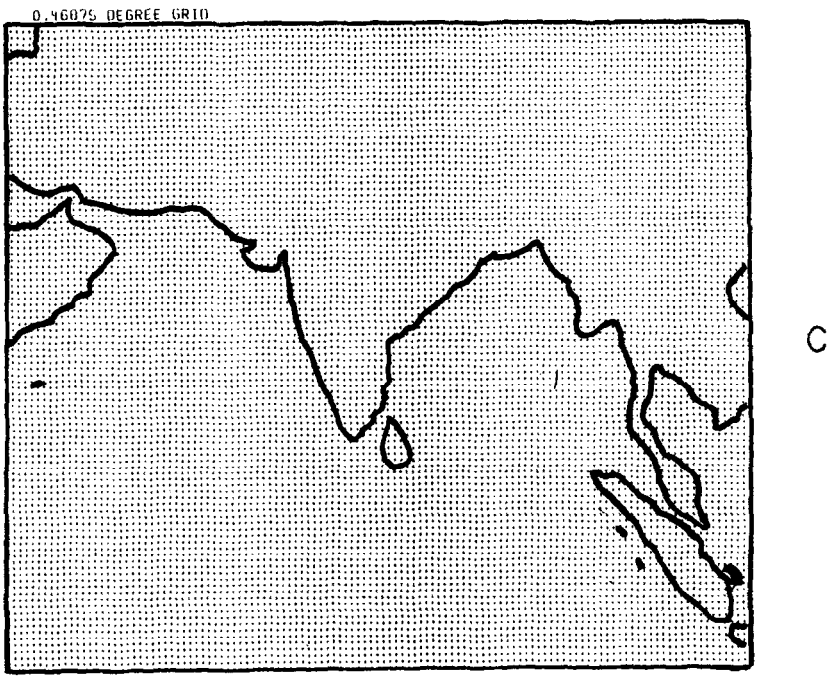

Fig. 1c.

Fig. 1. The grid points at the 1.875°, 0.938° and 0.469° resolution over the monsoon domain.

3. Parameterization of Ground Wetness

The proposed scheme is based on a moisture budget analysis, described by Yanai *et al.* (1983) and Haiyan He *et al.* (1987). Surface evaporation is estimated from a downward integration of the apparent moisture sink from the top of the atmosphere. The rainfall rates are provided from observations from raingauges and satellites. Using these evaporation rates, the surface energy balance equation is solved for surface temperature. Surface evaporation and surface temperature are then used to diagnose a ground wetness parameter from surface similarity theory.

The moisture continuity equation is expressed by:

$$\frac{\partial q}{\partial t} + \mathbf{V} \cdot \nabla q + \omega \frac{\partial q}{\partial p} = e - r \tag{3.1}$$

where

q = specific humidity;

$(\mathbf{V}, \omega)$ = horizontal wind vector and vertical velocity $\left[\frac{dp}{dt}\right]$

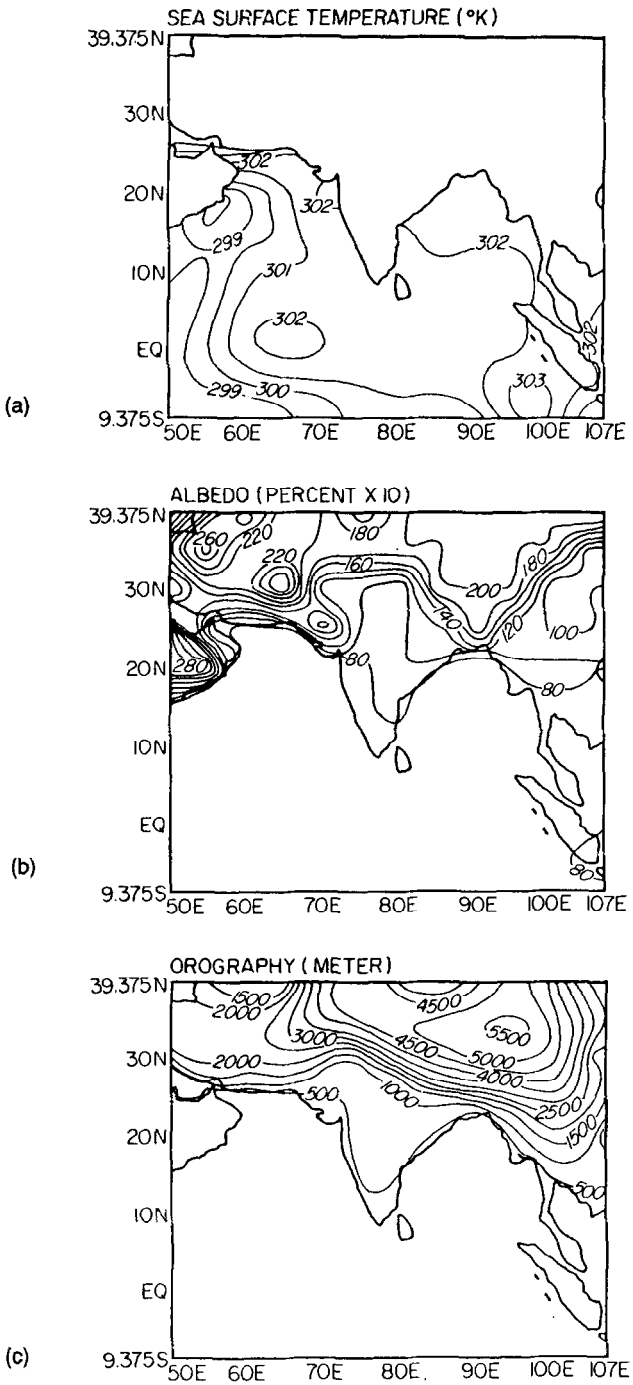

Fig. 2. (a) Sea surface temperature °K; (b) surface albedo; (c) terrain height (m), for the study period.

$$e = \text{vertical diffusion of moisture flux} = g\frac{\partial F_Q(p)}{\partial p}$$

where

$F_Q(p)$ = vertical moisture flux

r = moisture sink term, i.e. the condensation rate.

Integrating Equation (3.1) over the entire vertical column and upon multiplication by L/g, one obtains,

$$\frac{L}{g}\int_{p_T}^{p_s}\left[\frac{\partial q}{\partial t} + \mathbf{V}\cdot\Delta q + \omega\frac{\partial q}{\partial p}\right]dp = L[F_Q(p_s) - F_Q(p_T)] - \frac{L}{g}\int_{p_T}^{p_s} r\,dp \tag{3.2}$$

$$-\frac{1}{g}\int_{p_T}^{p_s} Q_2\,dp = LF_1 - LR \tag{3.3}$$

where

L = latent heat of vaporization

p_s = surface pressure

p_T = pressure at the top of the column taken as 125 mb, where the moisture is vanishingly small

Q_2 = apparent moisture sink

$$= -L\left[\frac{\partial q}{\partial t} + V\cdot\nabla q + \omega\frac{\partial q}{\partial p}\right]$$

R = Precipitation rate per unit area at the surface

$$= \frac{1}{g}\int_{p_T}^{p_s} r\,dP$$

F_1 = Surface evaporation per unit area = $F_Q(p_s)$

$F_Q(p_T)$ = vertical moisture flux at the top of the atmosphere which is assumed to be zero

We define LF_1 as the surface latent heat flux.

Equation (3.3) can be rewritten to provide surface latent heat flux as:

$$F_2 = LR - \frac{1}{g}\int_{p_T}^{p_s} Q_2\,dp. \tag{3.4}$$

Equation (3.4) is used to calculate F_2. For computing Q_2 from observed data sets, the horizontal wind components (u, v) and specific humidity from the FGGE level IIIB analysis are used. The vertical p-velocity ω is obtained from the horizontal divergence by integrating the continuity equation

$$\frac{\partial u}{\partial x} + \frac{\partial v}{\partial y} + \frac{\partial \omega}{\partial p} = 0 \tag{3.5}$$

with the surface boundary condition on ω at $p = p_s$ expressed by:

$$\omega = \omega_s = -g\,\rho_s\left[\frac{u_s}{a\cos\phi}\frac{\partial H}{\partial \lambda} + \frac{v_s}{a}\frac{\partial H}{\partial \phi}\right]. \tag{3.6}$$

This boundary condition incorporates orographic ascent.

$H = H(\lambda, \phi)$ specifies the surface terrain, where λ is the longitude and ϕ is the latitude, and u_s, v_s = surface zonal and meridional component of $\mathbf{V}$.

Assuming that the motion is approximately adiabatic near the tropopause, an additional condition is imposed on the vertical velocity ω at $p_T(\approx 125\text{ mb})$ from the thermodynamic equation, i.e.:

$$\omega = \omega_T = \frac{-\left[\dfrac{\partial \theta}{\partial t} + \mathbf{V}\cdot\nabla\boldsymbol{\theta}\right]}{\dfrac{\partial \boldsymbol{\theta}}{\partial \mathbf{p}}}. \tag{3.7}$$

This also follows the suggestion of Yanai *et al.* (1973); here θ is the potential temperature. Using these constraints the horizontal divergence is corrected as:

$$D^{\text{corrected}} = D^{\text{original}} + \frac{\omega_T - \omega_s - \displaystyle\int_{p_T}^{p_s} D^{\text{original}}\,dp}{p_s - p_T}. \tag{3.8}$$

Vertical velocity was calculated in this way by Krishnamurti and Sheng (1984) for the FGGE IIIb data sets.

After obtaining F_L, we coupled the surface energy balance and similarity theory in order to compute the ground wetness parameter (GW). To improve the accuracy of the solution, we adapted a soil-slab model for the surface energy balance. Following Blackadar (1979), we consider a thin surface soil layer at the surface temperature T_g in thermal contact with a deeper layer, which is assumed to be acting as a heat reservoir at constant temperature T_m:

$$C_g\frac{\partial T_g}{\partial t} = S_w^{\downarrow}(1-\alpha) + (L_w^{\downarrow} - \sigma T_g^4) - F_s^{\uparrow} - F_L^{\uparrow}$$

$$-C_g K_m(T_g - T_m). \tag{3.9}$$

The first term on the right-hand side of (3.9) is the net short-wave radiative flux

into the ground. The second term is the net long-wave radiative flux into the ground. The third and fourth terms are the upward sensible and latent heat fluxes. The last term is the flux due to conduction between the upper thin soil layer and the lower substrata. The surface albedo is given by α, while C_g and K_m are given by the following expressions (Blackadar, 1979),

$$C_g = 0.95(\lambda c_s/2\omega)^{\frac{1}{2}}$$

$$K_m = 1.18\omega$$

where c_s is the heat capacity of soil per unit volume = $\rho_g c_{sg}$, c_{sg} is the specific heat capacity of the soil, ρ_g is soil density, ω is the angular velocity of the earth's rotation and λ is the thermal conductivity of the soil. The heat capacity c_s and thermal conductivity λ are taken as functions of the moisture in the soil. For the present formulation, we have assumed c_s and λ to be linear functions of the soil moisture/ground wetness parameter GW, i.e.,

$$c_s = (1.42 + \mathrm{GW} * 1.68) * 10^6 \, J \, m^{-3} \, k^{-1} \tag{3.10}$$

$$\lambda = (0.25 + \mathrm{GW} * 1.33) \, W \, m^{-1} \, k^{-1}. \tag{3.11}$$

In the calculation of $(\partial T_g/\partial t)$, we have neglected surface cooling from falling rain.

The surface sensible heat flux F_s in Equation (3.9) is calculated using the following expression

$$F_s^{\uparrow} = \rho C_H C_p |\mathbf{V}_2|(T_2 - T_g), \tag{3.12}$$

where T_2 is the temperature at a chosen level within the constant flux layer at the surface, $\mathbf{V}_2$ is the horizontal wind vector at the same level, C_p is the specific heat and C_H is calculated using similarity theory. It is evident that in order to calculate C_H, knowledge of surface temperature is required. Therefore the flux equations are solved iteratively along with the equations for the similarity fluxes. $S_W^{\downarrow}$ and $L_W^{\downarrow}$ are calculated using the radiation algorithm of the FSU regional model; see Krishnamurti *et al.* (1990). F_L is obtained from F_2. Since c_s and λ depend on ground wetness, climatological values for GW are used as a first guess. For subsequent iterations, GW is updated using the procedure given below.

Once the surface temperature (T_g) is obtained, the surface saturation specific humidity q_{gs} is computed using Teten's formula. Given this surface temperature, the stability-dependent C_H and C_Q are calculated and the ground wetness parameter GW is estimated using the following formula:

$$\mathrm{GW}_Q = \frac{1}{q_{gs}} \left[q_2 - \frac{F_2}{\rho C_Q L |\mathbf{V}_2|} \right]. \tag{3.13}$$

This expression has been obtained by writing the latent heat flux F_L in a manner similar to the solution for F_s, i.e.,

$$F_L = \rho C_Q L |\mathbf{V}_2| (q_2 - \mathrm{GW} * q_{gs}). \tag{3.14}$$

The above equation is solved for GW, F_L replacing F_2. This generates a large data base for ground wetness from the vertically integrated moisture budget.

This GW is next expressed as a function of various large-scale variables. A selective second-order regression scheme is used to provide GW as a function of average 24 h accumulated rainfall rate, surface temperature, surface albedo, terrain, and surface humidity. In the regression, scaled albedo and scaled terrain heights are given by the relations,

$$\alpha' = \frac{(\alpha_{\max} - \alpha)}{(\alpha_{\max} - \alpha_{\min})} \tag{3.15}$$

$$H' = \frac{(H_{\max} - H)}{(H_{\max} - H_{\min})} \tag{3.16}$$

where $\alpha_{\max}$, $H_{\max}$ are maximum values of albedo and terrain. Similarly, $\alpha_{\min}$ and $H_{\min}$ are minimum values. In Table II, the coefficients of the multiple regression are presented. The regression has the form:

$$\begin{aligned}\mathrm{GW} = {} & a_0 + a_1 R + a_2 T_g + a_3 \alpha' + \alpha_4 H' + a_{11} R^2 + a_{22} T_g^2 + a_{33} \alpha'^2 + \alpha_{44} F'^2 \\ & + a_{12} R T_g + a_{13} R \alpha' + a_{14} R H' + a_{23} T_g \alpha' + a_{24} T_g H' + a_{34} \alpha' H'. \end{aligned} \tag{3.17}$$

TABLE II

The regression coefficients for GW in Equation (3.17)

a_0	3.131	a_4	−0.329
a_1	0.484	a_{11}	−0.130
a_2	−0.009	a_{33}	0.162
a_3	0.143	a_{44}	0.349

A pilot study using the above scheme was carried out with the FGGE IIIb data sets for the periods 11 May, 1979 through 16 May, 1979 and 20 June, 1979 to 28 June, 1979. Daily rainfalls were extracted from the Summer Monex experiment data sets, (Krishnamurti *et al.*, 1983). The domain chosen was 2.8°–38.4° N and 45.9°–113.4° E. The periods were selected to include heavy as well as light rainfall over different parts of the domain.

4. Sensitivity Studies

In this section, we shall compare the sensitivity of model predictions of ground wetness parameterizations for different horizontal resolutions and lateral boundary conditions.

The specific example we explore concerns the landfall of a tropical storm from the Bay of Bengal during the month of May. From several recent observational studies on low frequency modes on the time scale of 30 to 50 days, we have

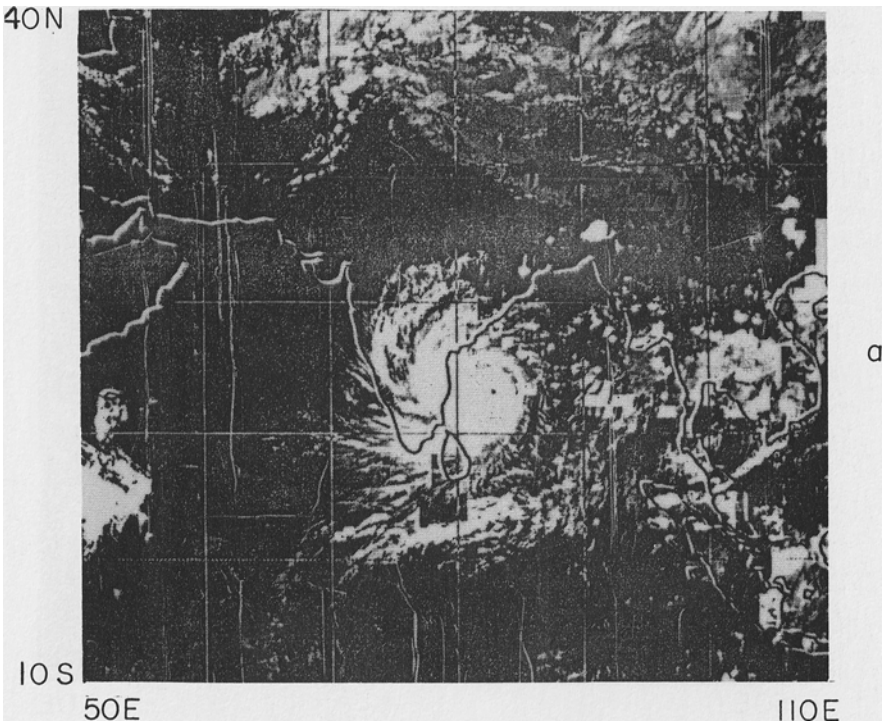

Fig. 3a. A DMSP infrared satellite photograph at 0300 UTC, May 12, 1979.

noted some interesting characteristics of these storms during the month of May (Krishnamurti and Subrahmanyam, 1982; Krishnamurti, 1985; Mehta and Krishnamurti, 1988) A family of zonally oriented cyclonic and anticyclonic eddies moves meridionally from roughly the equator to the Himalayas. This feature is evident during the northern summer months of the Asian summer monsoon. The waves have a meridional scale of roughly 300 km and move at a speed of roughly 1° latitude/day. The passage of a cyclonic eddy across 10° N during June coincides with the onset of the Indian monsoon along its southwest coast. This wave has its strongest amplitude over the Arabian Sea. The previous cyclonic wave of the low frequency family usually passes some 30 days earlier and has its strongest amplitude over the Bay of Bengal; its passage across 10° N coincides with the onset of the monsoon along the Burmese Coast. Within these cyclonic circulations of the low frequency waves, tropical storms form during the onset of the Burmese and the Indian monsoons during the months May and June, respectively. The Burmese onset usually follows a storm that generally moves in a westerly to a northerly direction affecting India or Bangladesh. The case study presented here is an example of one of the Burmese onset vortices (Krishnamurti *et al.*, 1981, 1990).

The satellite photographs shown in Figures 3a and 3b illustrate the banded spiral structure of the cloud cover of the tropical cyclone just prior to, and after landfall.

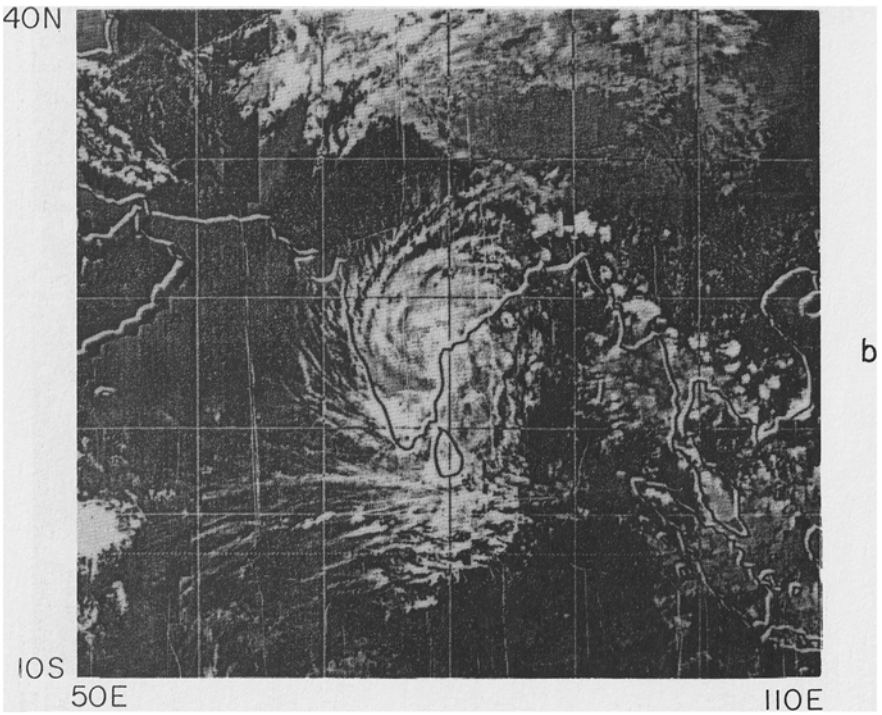

Fig. 3b. A DMSP infrared satellite photograph at 0300 UTC, May 13, 1979.

The dense cloud cover of the eye wall is also clearly portrayed. The observed rainfall amounts derived from roughly 3,000 raingauge sites suggest a banded pattern also in rainfall distribution, the highest amounts being of the order of 100 to 160 mm day^{-1} in the near coastal regions of southeastern India.

The observed storm circulation at 850 mb is illustrated in Figure 4a, b, c, corresponding to hours 0, 24 and 48 of the model forecasts. The wind field is based on the final ECMWF IIIb analysis. The data sets consist of the cloud-tracked winds from satellites over the ocean and the surface ship data from ships of opportunity. In addition, the coastal radiosonde-rawinsonde and the pilot balloon wind data form a part of the four-dimensional data assimilation. The slow westward propagation of the tropical cyclone over the Bay of Bengal is of particular interest. The ECMWF analysis was carried out on a 1.875° latitude/longitude mesh. At this resolution, the true intensity of the tropical cyclone is not analyzed. However, a circulation with winds of the order of 25 m s^{-1} is captured.

4.1. Results of initialization of surface fluxes

Figures 5a, b, c and 6a, b, c show sample calculations of the ground wetness parameterization during the premonsoon and postmonsoon onset periods, respectively. Panel (a) is based on the regression method. The results are nearly identical

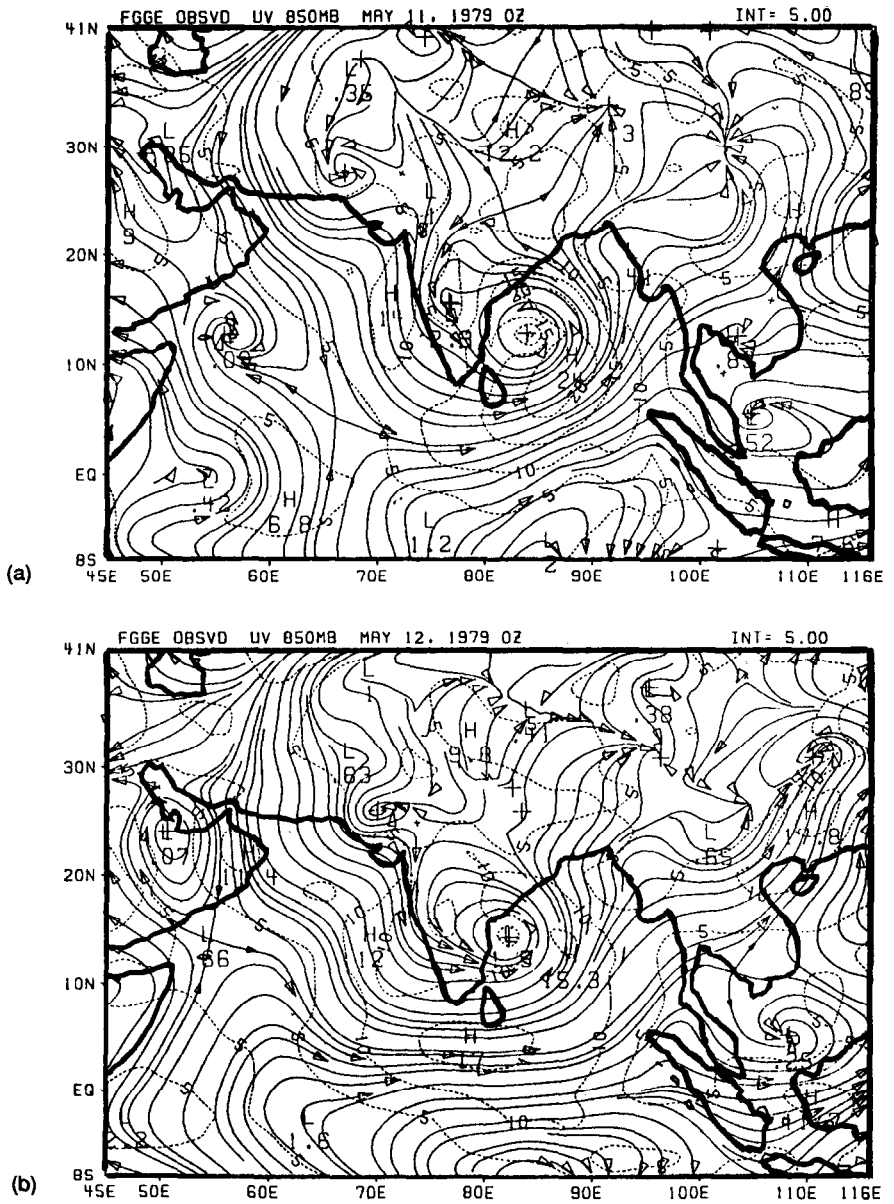

Fig. 4a, b.

to those obtained using the moisture budget. In comparison, the two simpler parameterizations of ground wetness based on surface albedo and surface relative humidity (b) and surface albedo alone (c) fail to show the details seen in panel (a). Of interest here is the region of southeastern India where the tropical cyclone makes its landfall, and where the ground wetness from the regression attains values close to 1.0, which are higher than the values given in panels (b) and (c).

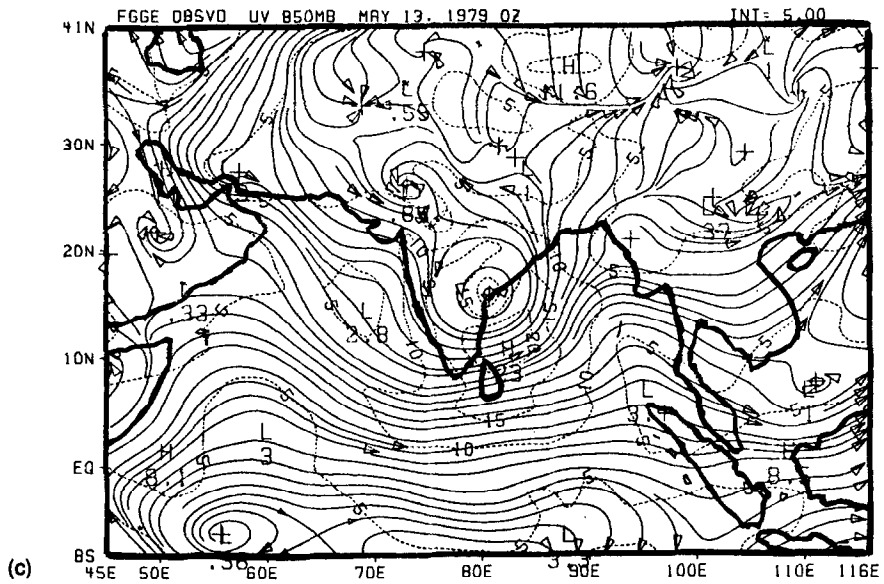

(c)

Fig. 4c.

Fig. 4a, b, c. Analysis of the wind field at 850 mb based on ECMWF's final IIIb. Streamlines (solid lines), isotachs m s^{-1} (dashed). Top panel day 0 i.e., May 11, 1979, 00z; middle panel day 1; bottom panel day 2.

The outer storm circulation interacts with the land region and appears to have a significant influence on the storm's landfall.

The surface temperature T_g over the land surface is obtained from a solution of the surface energy balance equation. Four versions of ground temperature are compared:

(a) From a solution of the surface energy balance where the surface moisture flux is assumed to be known from the vertical integral of Q_2 based on analysis of data sets.

(b) From a solution of the surface energy balance where the surface moisture flux is obtained from surface similarity theory using the regressed values of ground wetness.

(c) From a solution of the surface energy balance, with the surface moisture flux obtained from surface similarity theory with ground wetness as a function of surface albedo.

(d) From a solution of the surface energy balance, with surface moisture flux obtained from surface similarity theory with ground wetness as a function of surface albedo and relative humidity.

Figures 7 and 8 show the results for monsoon pre-onset and post-onset periods, respectively. We have undertaken such calculations for several such periods, and they all show that the bench-mark values of T_g based on the budgets of Yanai *et*

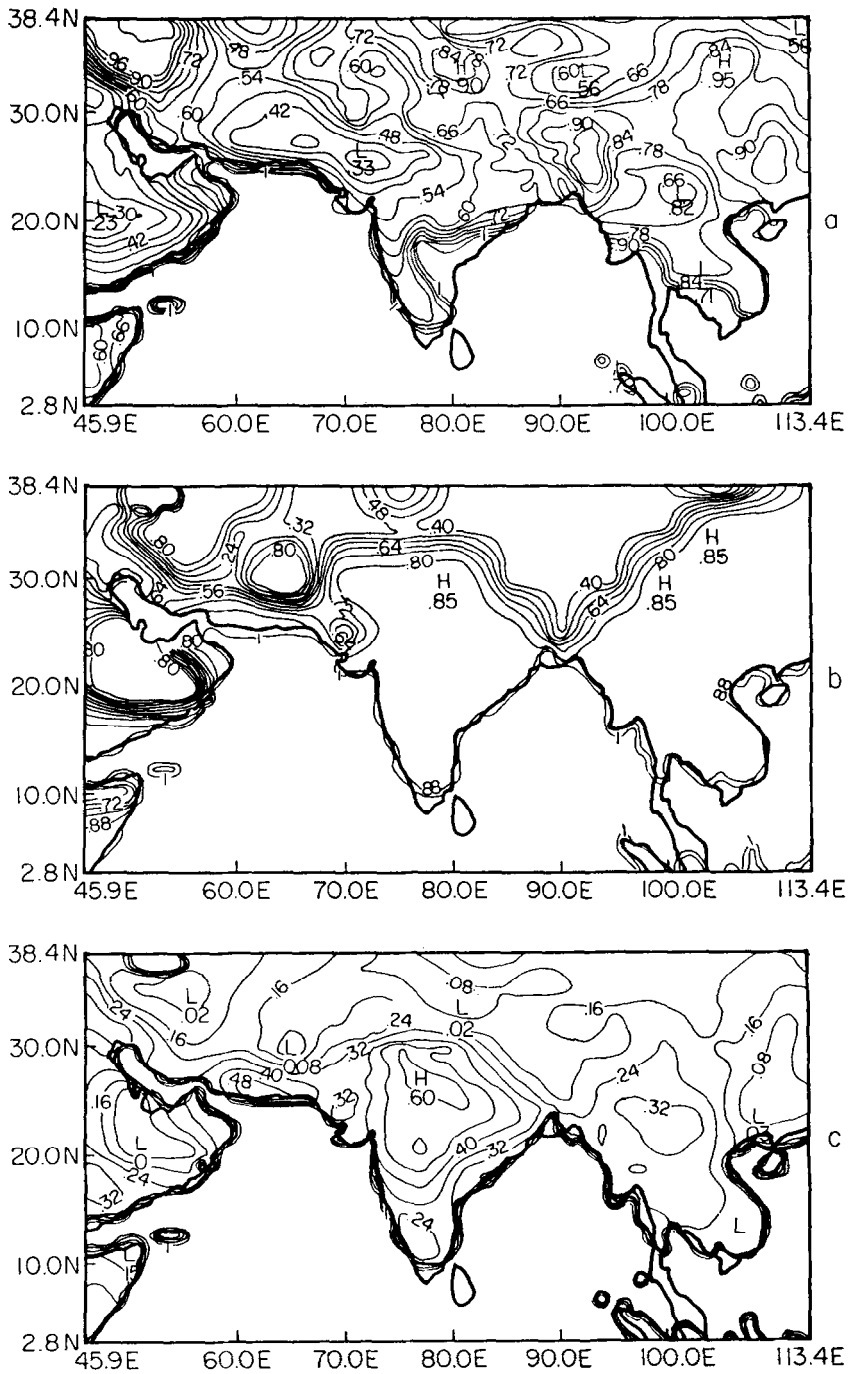

Fig. 5. The distribution of the ground wetness parameterization during a pre-monsoon onset period: (a) obtained from the regression method; (b) obtained from a parameterization of ground wetness as a function of surface albedo and surface relative humidity; (c) obtained from a parameterization of ground wetness as a function of surface albedo.

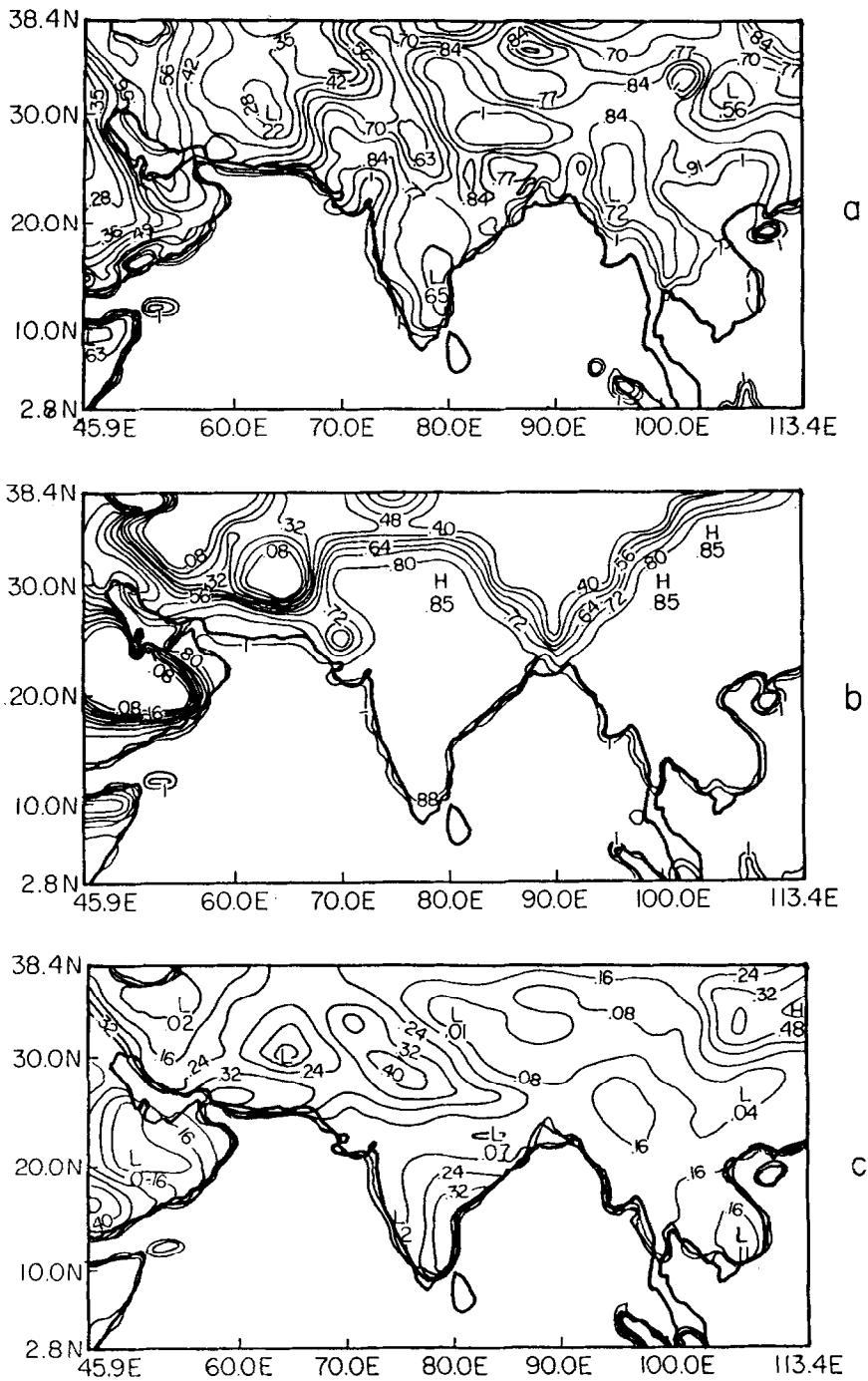

Fig. 6. The distribution of the ground wetness parameterization during a post-monsoon onset period: (a) obtained from the regression method; (b) obtained from a parameterization of ground wetness as a function of surface albedo and surface relative humidity; (c) obtained from a parameterization of ground wetness as a function of surface albedo.

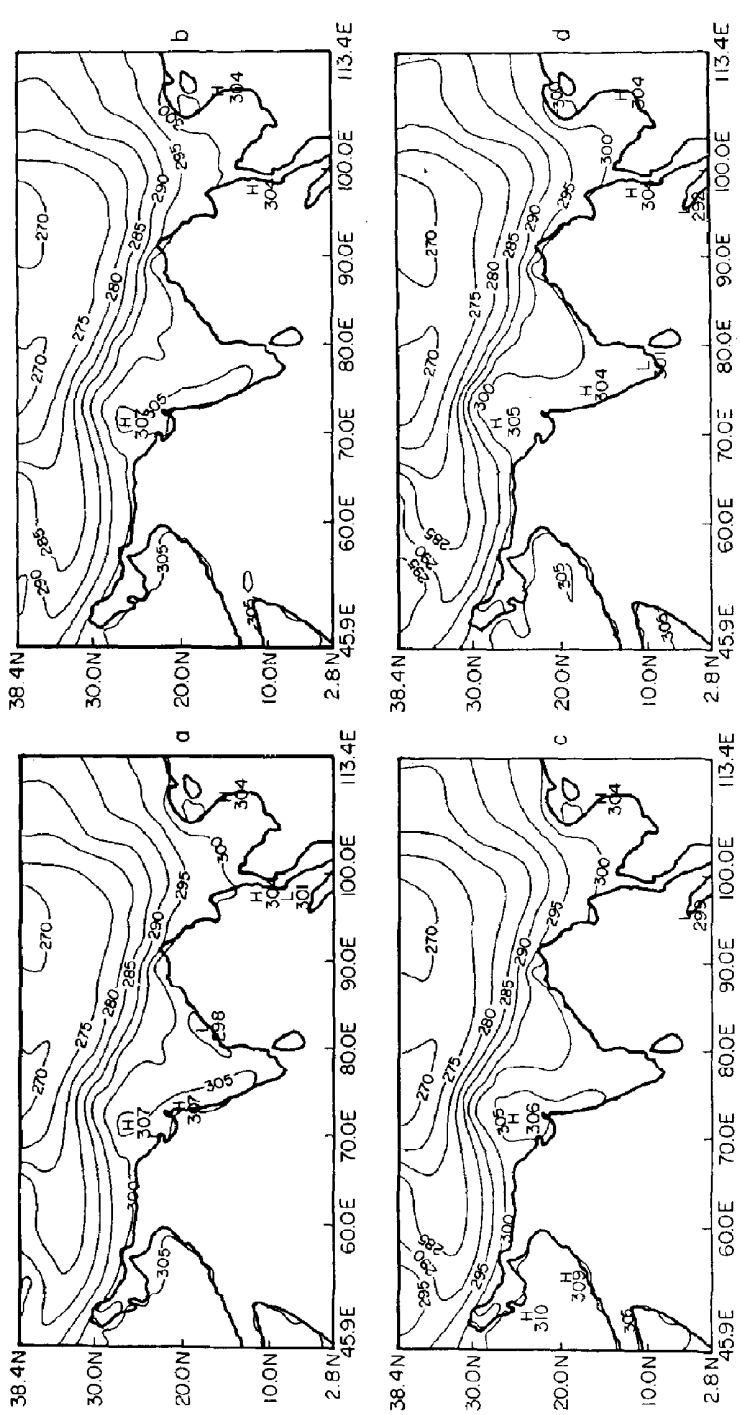

Fig. 7. Ground temperature calculation for a pre-monsoon onset case from the surface energy balance equation where: (a) ground wetness is based on a diagnostic moisture budget; (b) ground wetness is based on the improved method, i.e., regression; (c) ground wetness is a function of surface albedo; and (d) ground wetness is a function of albedo and surface relative humidity.

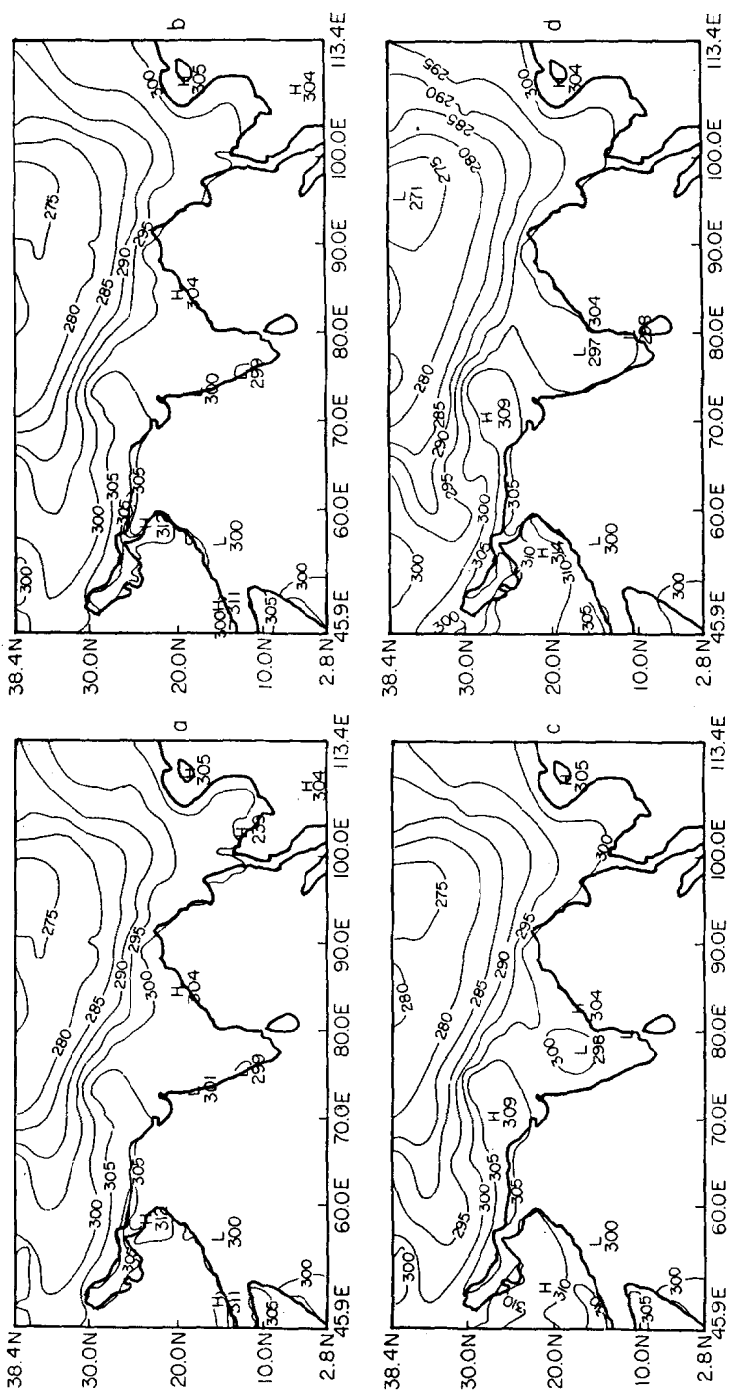

Fig. 8. Ground temperature calculation for a post-monsoon onset case from the surface energy balance equation where: (a) ground wetness is based on a diagnostic moisture budget; (b) ground wetness is based on the improved method, i.e., regression; (c) ground wetness is a function of surface albedo; and (d) ground wetness is a function of albedo and surface relative humidity.

al. (1973) (panel (a)) are closely reproduced by the regression-based parameterization of ground wetness (panel (b)). Panels (c) and (d) show poor agreement with panel (a).

Figures (9a, b, c and d) and (10a, b, c and d) illustrate the calculations for pre-monsoon and a post-monsoon onset period, of the surface latent heat flux obtained as follows:

Panel (a) The diagnostic moisture budget method, i.e., from a vertical integration of Q_2.
Panel (b) The surface fluxes obtained from the proposed regression method.
Panel (c) The surface fluxes obtained from ground wetness as a function of surface albedo.
Panel (d) The surface fluxes obtained from ground wetness as a function of surface albedo and surface relative humidity.

In both Figures 9 and 10, the regression-based initialization recovers the fluxes of Yanai *et al.* (1973) very closely. That is not the case for the parameterization based on surface albedo and on surface relative humidity and surface albedo. The key ingredient in this improvement is the inclusion of rainfall for the past 24 hours within the parameterization of ground wetness.

In a control experiment, the ground wetness was simply expressed as a function of the prescribed surface albedo. According to this formulation, the ground wetness has a strong inverse relationship to surface albedo. In the parameterized ground-wetness experiment, the statistical relation, described in Section 3, was used. Otherwise these two sets of experiments were identical, including data sets and initial states. In a two- to three-day prediction experiment, we do not expect a large impact from the parameterization of land surface processes. That is more of a climate issue as has been demonstrated by Yamakazi (1989) and several others. Basically, these studies show an improvement in climatological rainfall patterns with a time-dependent modeling of ground wetness. A reduction in soil moisture causes a reduction in evaporation which in turn is shown to reduce the rainfall amounts in these studies. A motivation for carrying out the proposed comparisons is to see if the parameterization scheme is stable and if it shows any measurable changes in the precipitation estimates within the considered time frame.

The other aspect of experimentation covered in this section concerns the combined effects of resolution and ground wetness parameterization on the prediction. The increase of resolution does have a direct effect on the increase of vertical motion and rainfall rates. The increased rainfall provides an enhancement of the ground wetness parameterization and a positive feedback via latent heat fluxes. This can lead to a further increase in rainfall.

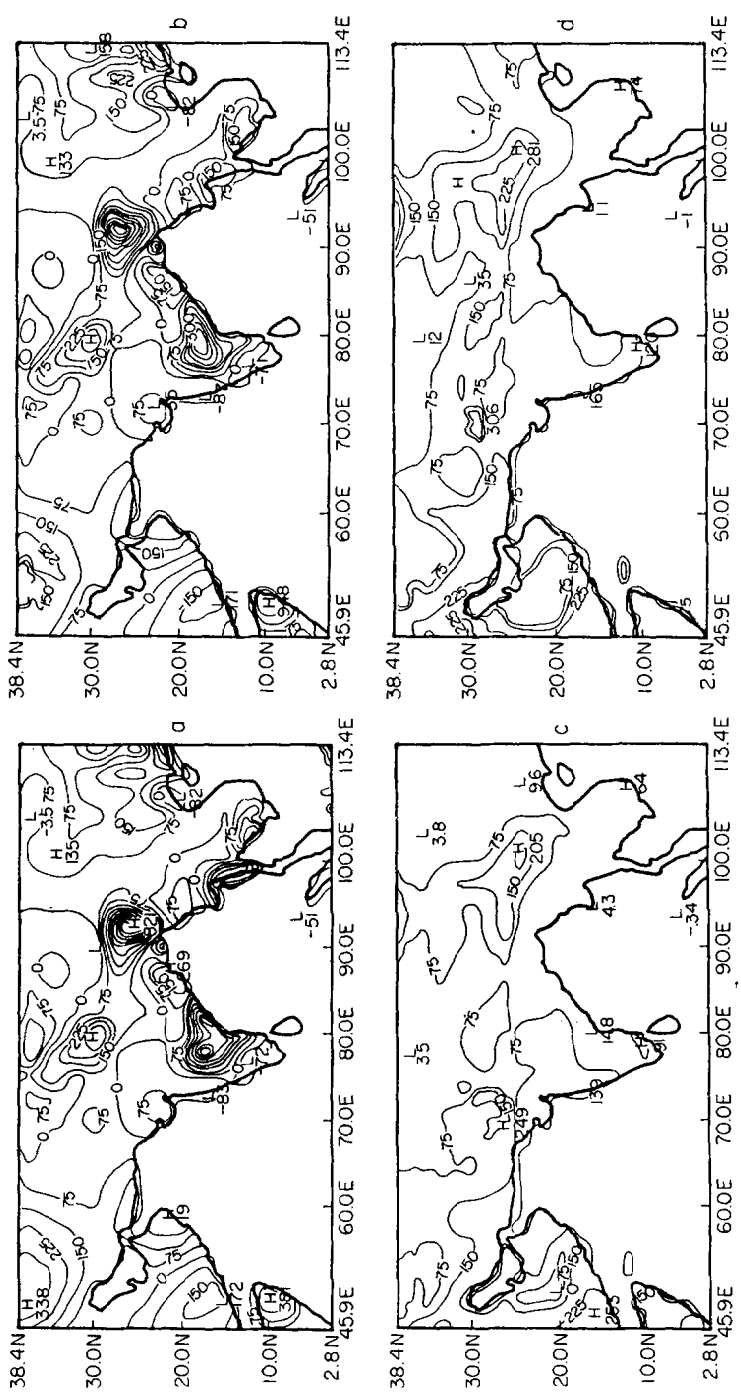

Fig. 9. Surface flux of latent heat (W m^{-2}) (pre-monsoon onset case): (a) based on a diagnostic moisture budget; (b) based on ground wetness obtained from a regression; (c) based on ground wetness expressed as a function of surface albedo; and (d) based on ground wetness expressed as a function of surface albedo and surface relative humidity.

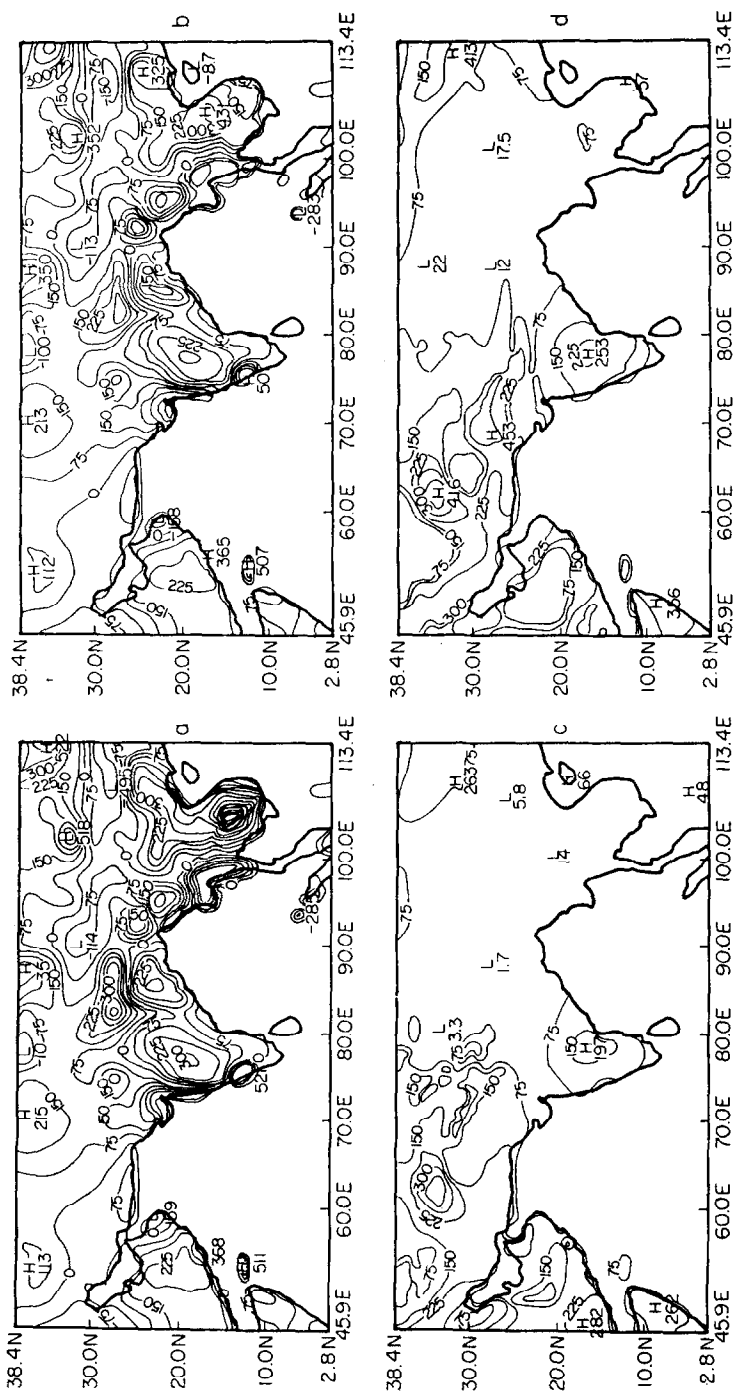

Fig. 10. Surface flux of latent heat (W m^{-2}) (post-monsoon onset case): (a) based on a diagnostic moisture budget; (b) based on ground wetness obtained from a regression; (c) based on ground wetness expressed as a function of surface albedo; and (d) based on ground wetness expressed as a function of surface albedo and surface relative humidity.

4.2. Rainbands

The spiral rainbands occurring in hurricanes have been studied for a number of years. In the context of numerical weather prediction models, the simulation of the convection along the spiral rainbands, and along the eye wall of a hurricane, is recognized as a problem of major interest.

Three-dimensional hurricane forecasting (or simulation) studies began with the efforts of Anthes *et al.* (1972) and Miller *et al.* (1972). In recent years, Yamasaki (1986, 1989) has described some of the major developments in the simulation and prediction of hurricanes including their rainbands and the eye-wall. These recent improvements include the development of a new cumulus parameterization scheme. Yamasaki (1975) developed a non-hydrostatic cloud ensemble model within a prescribed large-scale environment. By carrying out three-dimensional integrations in such a model, Yamasaki generated the heating, moistening, and rainfall rates by the cloud ensemble as functions of prescribed large-scale conditions. With the data sets thus generated, he developed a cumulus parameterization scheme for tropical numerical weather prediction. This led to the successful simulation of hurricanes with realistic structures (Yamasaki, 1986, 1989). These studies showed the existence of a large frictional control in the formation of the rainbands of a hurricane. The inflow angle of the spiral bands, and the number of bands, seem to be controlled by the specification of surface-layer physics, based in Yamasaki's studies on conventional bulk-aerodynamic formulae. Our present modeling effort utilizes similarity theory in the surface constant-flux layer. The surface exchange coefficients are stability dependent.

The predicted rainfall fields for the first and second 24 hours are shown in Figures 11 and 12. Figure 11a, b illustrate the results from the use of 'perfect' boundary conditions, (i.e., based on an analysis of observations), 0.4687° resolution and the improved ground wetness parameterization. These were the best results in this series of experiments. The banded structure of the precipitation patterns for the first and second day bear a close resemblance to the bands of the satellite imagery shown in Figure 3a, b. The rainfall amounts along the bands are of the order of 20 to 50 mm day^{-1}, while in the interior region of the storm, near its center, the rainfall amounts exceed 100 mm day^{-1}. Raghavan (1990) examined radar PPI-scope projections of several Bay of Bengal storms and noted that rainfall bands preserve their structure over the land as a storm approaches the coastline.

When the 'perfect' boundary conditions are replaced by those provided by a global model (T106) (Figure 12) forecast, the bands are still reasonably predicted although some of the details are degraded. In particular, the extension of rain bands into the southern Arabian Sea is not predicted. Overall, the intensity and number of bands are underestimated. It appears that forecast errors at the boundaries, from the global model, degrade the forecasts of the higher resolution regional model. The storm's phase speeds for this experiment were somewhat slower than those of the 'perfect' boundary experiment. The phase speed error has possibly contributed to the diminished activity over the Arabian Sea. The

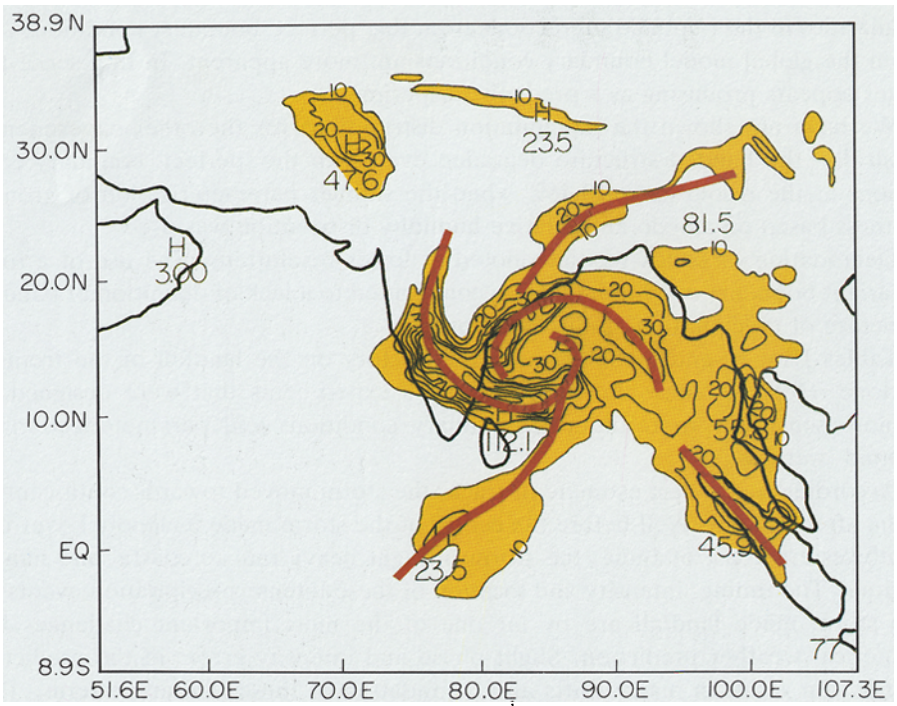

Fig. 11a. Predicted rainfall for hours 0 to 24 mm day^{-1}. 0.469° mesh, perfect boundary conditions and improved parameterization of ground wetness.

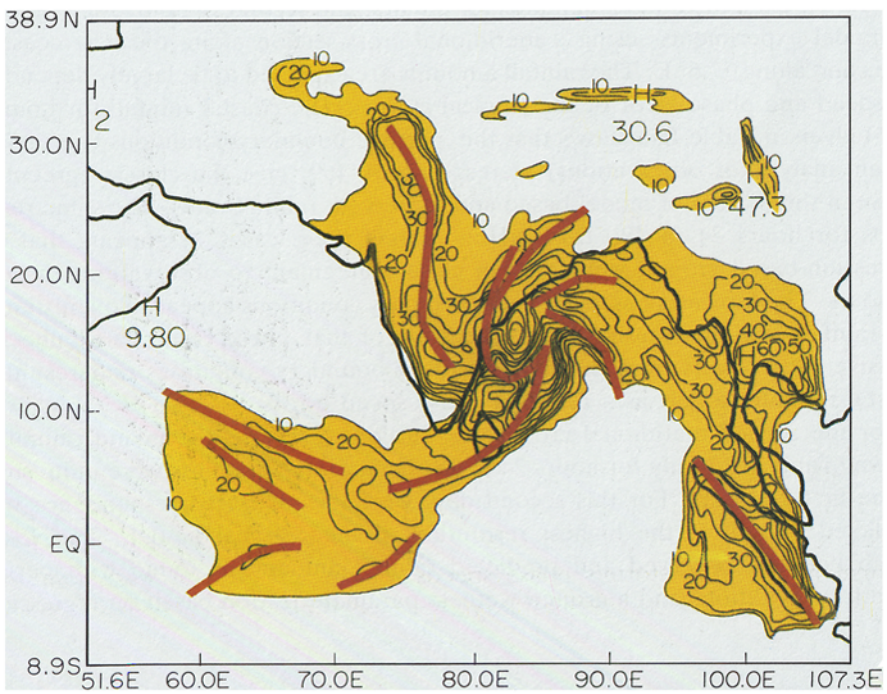

Fig. 11b. Predicted rainfall for hours 24 to 48 mm day^{-1}. 0.469° mesh, perfect boundary conditions and improved parameterization of ground wetness.

similarities in the rainband predictions from the 'perfect' boundary conditions and from the global model boundary conditions are more apparent. In that sense the latter appears promising as a predictive experiment.

We have not shown the precipitation distributions for the other experiments. Basically, the banded structure degraded even with the 'perfect' boundary conditions at the resolution of 0.469° when the simpler parameterization of ground wetness based on albedo and relative humidity distribution was used.

Degradation of bands was also noted at lower resolutions. The use of a time invariant boundary condition likewise contributed to a lack of definition of banded structure of precipitation at all resolutions.

Tables IIIa, b, and c contain a rainfall history on the landfall of the tropical cyclone. Here we show the results from 10 experiments that were designed to explore sensitivity to resolution, boundary conditions and parameterization of ground wetness.

According to the best estimate of track, the storm moved towards south-central India after landfall. Well before the center of the storm made its landfall over the southwestern coast of India, the storm brought heavy rain to coastal and inland regions. The timing, intensity and location of these intense precipitation events as the storm made landfall are by far one of the most important challenges for numerical weather prediction. Slight phase and intensity errors in the predicted storms can result in major shifts and degradation of these rainfall patterns. The sensitivity experiments, presented here, provide measures of the coastal and the inland rainfall amounts.

Here we examine rainfall amounts for the first and second 24 hours for a number of model experiments, using a meridional cross-section along the east coast of India and along 77.5° E. The rainfall amounts are expected to be largely dependent on speed and phase error of the tropical storms. The coastal rainfall for hours 0 to 24 given in Table IIIa shows that the 'perfect' boundary conditions (i.e., based on an analysis of observations) at resolution 0.469° give the closest agreement between three cases of model-based and 'observed' rainfall rates. The same result holds for hours 24 to 48, Table IIIb. Among these cases, it appears that the regression-based ground wetness is in closer agreement to observations through 48 hours. The forecasts based on T106 boundary conditions appear to overestimate the rainfall amounts south of 15° N; in spite of that, these results are quite impressive. The results from the time-invariant boundary conditions underestimate coastal rainfall, largely as a result of phase speed errors.

For the second meridional cross-section (along 77.5° E), the inland rainfall is shown (Table IIIc) only for hours 24 to 48 since rainfall amounts were quite small in the first 24 hours. For this second day, we note a close correspondence with predicted rainfall at the highest resolution of the regional model. The closest match between observed and predicted rainfall amounts is found with perfect boundary conditions and a ground wetness parameterization based on regression.

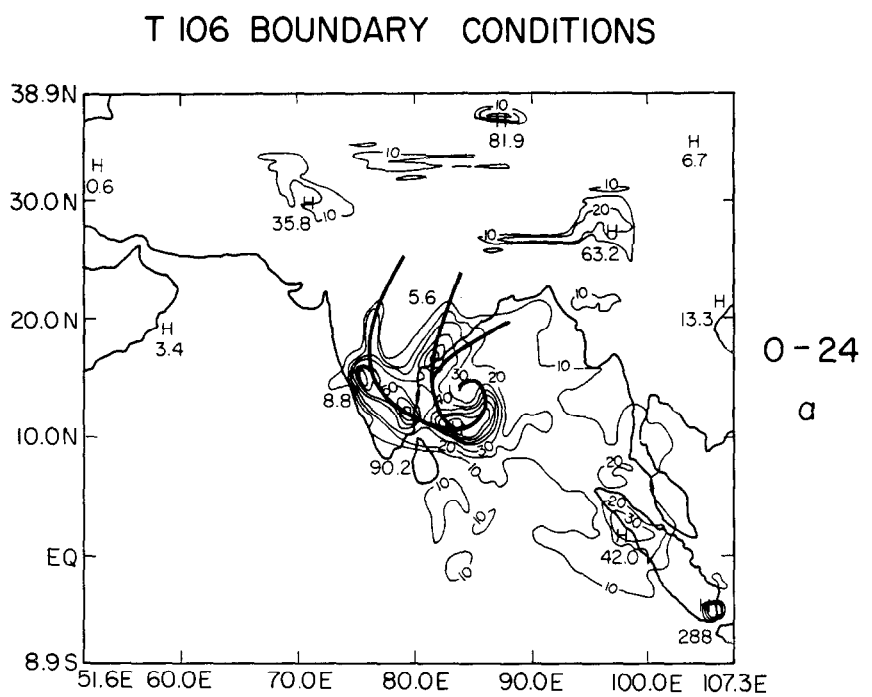

Fig. 12a. Predicted rainfall for hours 0 to 24 mm day^{-1}. 0.469° mesh, global model (T106) boundary conditions, improved parameterization of ground wetness.

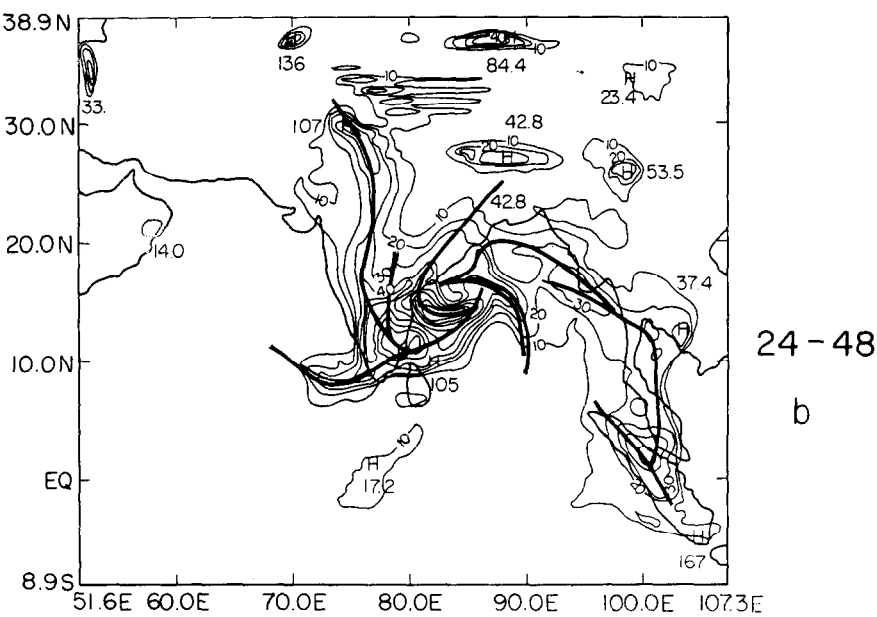

Fig. 12b. Predicted rainfall for hours 24 to 48 mm day^{-1}. 0.469° mesh, global model (T106) boundary conditions, improved parameterization of ground wetness.

TABLE IIIa

Coastal rainfall (east coast of India) mm day^{-1} hours 0 to 24

Latitude — °N			0	2.5	5	7.5	10	12.5	15	17.5	20	22.5	25
Observed (raingauge) satellite		Averaged over 1° square	–	–	–	–	57	115	75	40	10	5	–
Resolution	Boundary conditions	Ground wetness	Rainfall from different model experiments										
1.875	Analysis of observations	R.H.	–	–	–	–	18	21	23	29	12	3	–
1.875	–	R.H., albedo	–	–	–	–	19	22	26	30	10	4	–
0.938	–	R.H., albedo	–	–	–	–	10	22	9	11	5	8	–
0.938	–	Regression	–	–	–	–	28	28	21	25	10	18	–
0.938	Time invariant	R.H., albedo	–	–	–	–	4	12	15	10	6	5	–
0.469	Analysis of observations	R.H.	–	–	–	–	51	74	180	65	31	22	–
0.469	–	R.H., albedo	–	–	–	–	55	71	191	71	25	21	–
0.469	–	Regression	–	–	–	–	95	60	75	90	18	8	–
0.469	T106	–	–	–	–	–	30	41	42	10	11	8	–
0.469	Time invariant	–	–	–	–	–	15	21	18	12	7	3	–

TABLE IIIb

Coastal rainfall (east coast of India) mm day^{-1} hours 24 to 48

Latitude – °N			0	2.5	5	7.5	10	12.5	15	17.5	20	22.5	25
Observed (raingauge) satellite		Averaged over 1° square	–	–	–	–	8	41	64	31	6	5	–
Resolution	Boundary conditions	Ground wetness	Rainfall from different model experiments										
1.875	Analysis of observations	R.H.	–	–	–	–	19	22	32	40	16	14	–
1.875	–	R.H., albedo	–	–	–	–	24	38	37	41	17	14	–
0.938	–	R.H., albedo	–	–	–	–	65	77	60	52	20	41	–
0.938	–	Regression	–	–	–	–	28	35	45	40	25	4	–
0.938	Time invariant	R.H., albedo	–	–	–	–	0	7	8	11	6	2	–
0.469	Analysis of observations	R.H.	–	–	–	–	14	12	45	40	31	18	–
0.469	–	R.H., albedo	–	–	–	–	17	19	41	37	39	12	–
0.469	–	Regression	–	–	–	–	32	65	66	37	51	11	–
0.469	T106	–	–	–	–	–	59	61	62	43	31	8	–
0.469	Time invariant	–	–	–	–	–	24	29	18	18	17	10	

TABLE IIIc

Inland rainfall (along 77.5°E) mm day^{-1} hours 24 to 48

Latitude – °N			0	2.5	5	7.5	10	12.5	15	17.5	20	22.5	25
Observed (raingauge) satellite		Averaged over 1° square	10	14	18	10	5	18	60	25	5	2	0
Resolution	Boundary conditions	Ground wetness	Rainfall from different model experiments										
1.875	Analysis of observations	R.H.	0	2	4	12	19	30	24	15	6	4	0
1.875	–	R.H., albedo	0	3	7	13	19	29	30	12	7	2	0
0.938	–	R.H., albedo	0	5	7	8	32	15	8	7	7	8	8
0.938	–	Regression	0	5	6	3	10	23	11	4	2	3	2
0.938	Time invariant	R.H., albedo	0	0	3	12	10	16	12	11	4	2	1
0.469	Analysis of observations	R.H.	6	11	20	45	40	53	39	28	20	9	21
0.469	–	R.H., albedo	10	18	21	48	41	50	38	24	21	11	15
0.469	–	Regression	23	11	8	9	10	41	55	32	20	8	5
0.469	–	T106	0	0	0	5	10	22	88	21	20	8	8
0.469	Time invariant	–	0	0	0	0	4	11	10	2	1	0	0

The forecasts based on global model boundary conditions also appear to be quite close to the 'observed' measures north of 10° N.

Overall, it appears that the ground wetness parameterization seems to affect the outer storm circulation. In the absence of boundary errors, an improved parameterization of ground wetness leads to an improvement in prediction skill.

4.3. A HIGH RESOLUTION GLOBAL MODEL FORECAST

We have carried out a parallel forecast with a global model at resolution T106. The grid point separations at this resolution are roughly 100 km over the tropics. That is less than the highest resolution of the regional model used in the present study. The difference in resolution also has an impact on the representation of orography. However, the parameterization of physical processes in the global and the regional model are nearly identical. It is of interest first to examine the precipitation patterns predicted by the global model; see Figure 13a, b, respectively. The patterns do not reveal the detailed structure, as does the high resolution regional model. Next we look at the storm position at hours 24 and 48 predicted by the global model (at resolution T106) and find that it was within 100 km of the best track position. The global model predicted coastal rainfall quite well at both hours 24 and 48; however, inland rainfall was underestimated.

It is of considerable interest to note that although the detailed structure of the storm was not reasonably predicted by the global model, the model does provide boundary conditions to the higher resolution regional model which seems to perform slightly better than the global model. A comparison of the 24- and 48-hour rainfalls in Figures 12 and 13 illustrates this. Thus it appears that a global model, run at a slightly lower resolution, can provide useful boundary conditions for a higher resolution regional model.

4.4. TROPICAL CYCLONE TRACK

Some of the cyclone tracks are displayed in Figure 14, where horizontal resolution and boundary conditions are given at the top left of each diagram. It is worth noting that well prior to landfall, the outer storm circulation and the outer rainfall interact with the underlying surface; this seems to affect storm behavior and position at about the time of the landfall. The simpler version of the ground wetness parameterization, which is a function of surface albedo and relative humidity, shows a broad belt of large ground wetness exceeding 0.8 over the entire Indian peninsula, Figures 5 and 6. This resulted in a broad region of weaker inland rainfall. In contrast, when the pattern of ground wetness exhibited low and high values on scales smaller than the Indian peninsula, the heavier inland rainfall tended to remain more confined to regions of higher ground wetness, thus preserving the sharper banded features. Increased surface roughness of the land area and a uniformly large ground wetness seems to break up the banded pattern. In Table IV, we present predicted positions of the storm centre for a limited sample of 8 experiments. The following general inferences can be drawn.

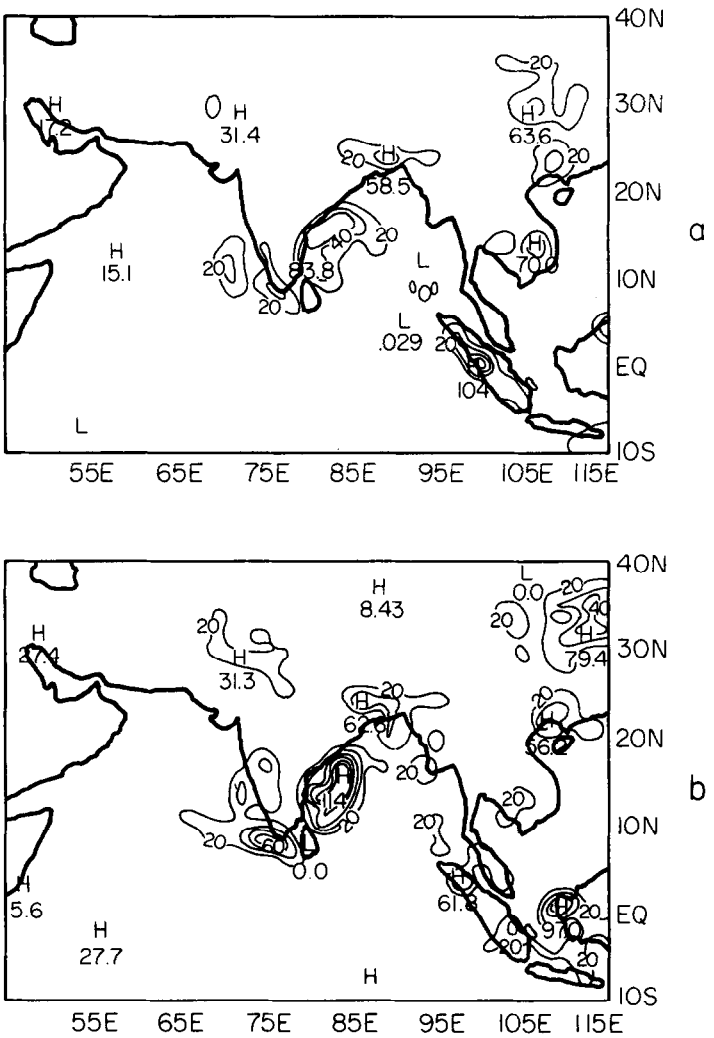

Fig. 13a, b. Predicted rainfall mm day^{-1} from the global model at resolution T106. Top panel, forecast for hours 0 to 24; bottom panel, forecast for hours 24 to 48, day 0 is May 11, 1979 00 UTC.

(a) The best results, in terms of 48-hour track forecasts, were obtained when 'perfect boundary conditions' were used at the highest resolution (0.469° lat/long) and with ground wetness parameterization based on the regression.

(b) For decreasing resolution, for both the 'perfect boundary conditions' and the 'regression' version of ground wetness, track forecast errors increased.

(c) The use of fixed boundary conditions produced the largest errors in track forecasts.

(d) The global model (at resolution T106) produced a track forecast error which was larger than in (a) above. The resolution and parameterization of ground wetness were identical to those in (a). The 48-hour forecast position error

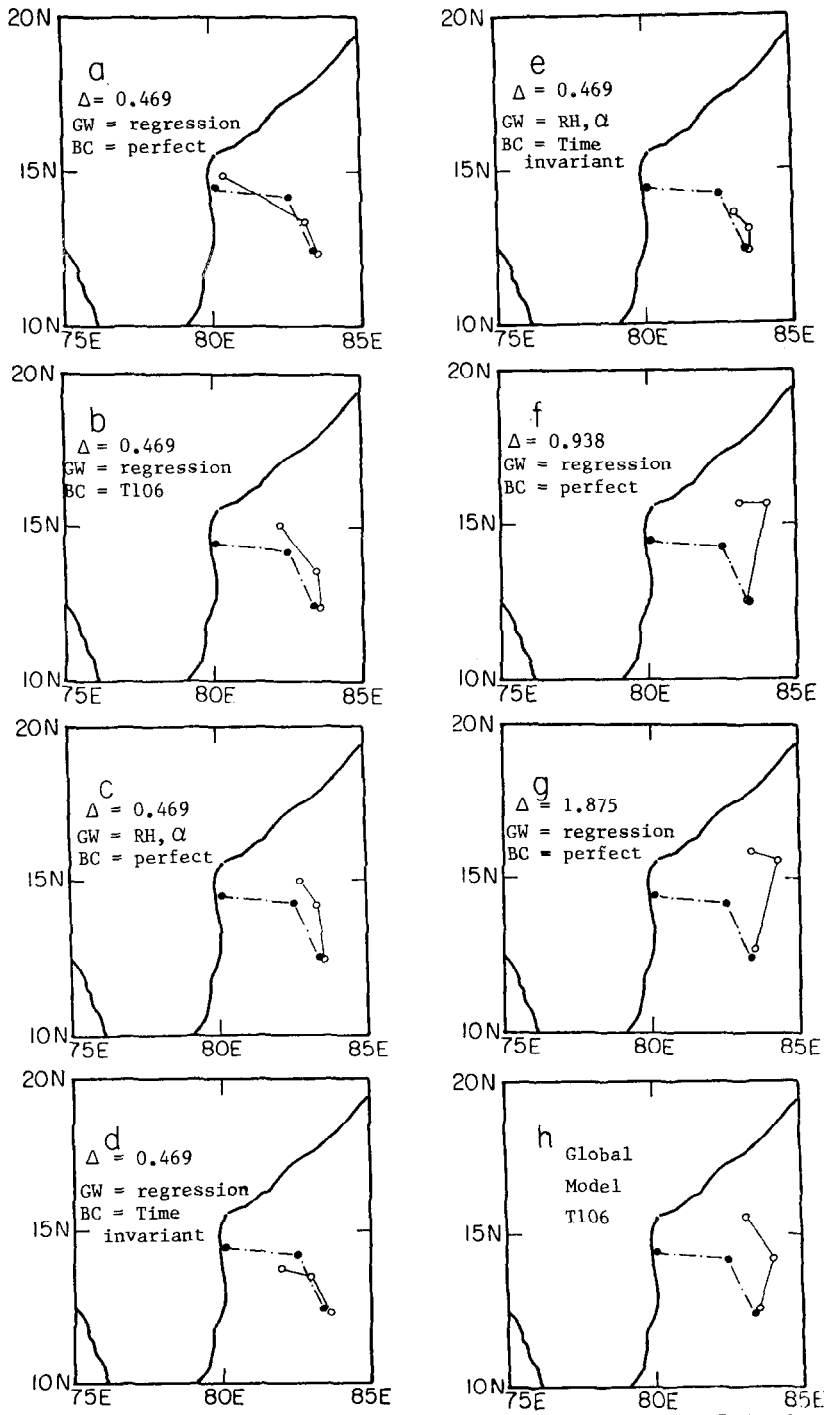

Fig. 14. Storm track between hours, 0, 24 and 48. Legend: Δ = grid resolution; B.C. = boundary conditions; α = albedo; R.H. = relative humidity; and G.W. = ground wetness.

TABLE IV

Predicted positions of storm centre

Exp. No.	Horizontal resolution	Boundary conditions	Ground wetness	Forecast time 0 Lat.	0 Long.	24 hr Lat.	24 hr Long.	48 hr Lat.	48 hr Long.
1	0.469	Perfect	Regression	12.3° N	83.5° E	13.2° N	83.1° E	14.8° N	81.5° E
2	0.469	T-106	Regression	12.3° N	83.5° E	13.5° N	84.5° E	15.0° N	82.2° E
3	0.469	Perfect	RLH, α	12.3° N	83.5° E	14.1° N	83.2° E	14.9° N	82.8° E
4	0.469	Fixed	Regression	12.3° N	83.5° E	13.6° N	82.9° E	13.9° N	82.0° E
5	0.469	Fixed	RH, α	12.3° N	83.5° E	13.1° N	83.5° E	13.6° N	83.0° E
6	0.938	Perfect	Regression	12.6° N	83.3° E	15.6° N	84.0° E	15.7° N	83.1° E
7	1.875	Perfect	Regression	12.6° N	83.4° E	15.5° N	84.2° E	15.8° N	83.3° E
8	T106	A global model	α	12.5° N	83.5° E	14.2° N	84.0° E	15.5° N	83.1° E
	1.875°	Based on ECMWF analysis	Based on ECMWF analysis	12.4° N	83.2° E	14.1° N	82.5° E	14.4° N	80.1° E

for the best experiment (with perfect boundary conditions) was of the order of 110 km as compared to roughly 180 km for this experiment (T106 boundary conditions).

(e) The results for a straight run with the global model at the resolution T106 are also presented in this table. This shows a position error of the order of 180 km for the 48 hour forecast.

(f) The use of a ground wetness parameterization based on surface relative humidity and albedo led to slightly larger track forecast errors compared to the regression-based ground wetness parameterization.

We also ran an experiment through 72 hours starting on May 11, 1979 00 UTC with very dry soil conditions. The ground wetness parameter over the entire peninsular India, south of 20° N, was artificially set to 0.1. The tropical cyclone moved westward and stalled near 80° E and dissipated by day 3 near the coastal region. This behavior was similar to that of a monsoon onset vortex in the Arabian sea (Krishnamurti *et al.*, 1981, 1984). The Arabian sea vortices usually dissipate near the Arabian coast, without any inland penetration into the desert region.

As an example, Figure 15 shows one of the circulation forecasts at the 850 mb level, using perfect boundary conditions at resolution 0.49° and the improved version of the ground wetness parameterization. This was one of the better forecasts in terms of storm track, the circulations shown here agreeing closely with those presented in Figures 4b and 4c. Phase errors of the storm center were quite large in several other experiments where the circulations were generally displaced towards the ocean; this is evident from Table IV.

The regional model at high resolutions seems to be the more appropriate model

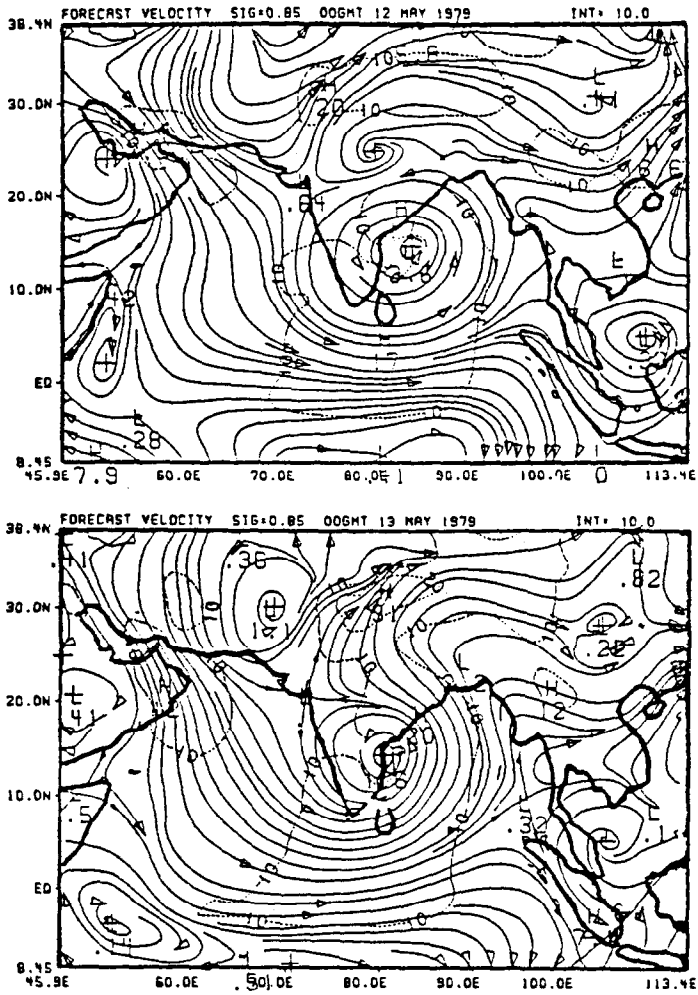

Fig. 15a, b. Predicted wind field at 850 mb. Top panel 24-hour forecast; bottom panel 48-hour forecast; streamlines and isotachs (dashed lines, m s^{-1}); day 0 is May 11, 1979 00 UTC.

for studying regional weather – such as the landfall of a hurricane. However, that issue is not entirely settled by this study. The choice of 'perfect' boundary conditions appears to provide the best results. That level of accuracy in the structure and motions of the storm is not attained from a global model (T106). This global model had a transform grid separation of roughly 100 km. One might try boundary conditions from a global model at a resolution such as T200, which would have a transformed grid separation comparable to the resolution of the regional model. It is likely that the global model at that resolution would perform as well as a regional model at comparable resolution. If that were so, the use of the global model's boundary conditions would seem to be redundant.

5. Concluding Remarks

Some useful model predictions on precipitation patterns associated with a tropical cyclone during its landfall have been obtained from a high-resolution regional numerical prediction model (Krishnamurti *et al.*, 1990). The predicted spiral rainbands and the eye-wall rainfall show close agreement with raingauge measurements. The overall rainfall patterns agree closely with the DMSP imagery obtained from a high resolution satellite. We have explored the sensitivity of the landfall forecasts to three variables: lateral boundary conditions, horizontal resolution and ground wetness parameterization. We find reasonable agreement between observations and model predictions when using 'perfect' (i.e., based on analysis of observations) boundary conditions, a horizontal resolution of the order of 50 km and an improved ground wetness parameterization based on past rainfall, surface albedo and surface relative humidity. Predictions of rainband structure, storm rainfall and storm position at hour 48 are not so good for other resolutions, ground wetness parameterizations and boundary conditions. In a predictive sense, the use of boundary conditions from a global model would seem logical. However, it appears that one has to run a fairly high resolution global model in order to provide such boundary conditions. Thus it is not clear whether such a high resolution global model might itself serve the purpose in providing adequate forecasts.

The ground wetness parameterization appears to influence the storm's landfall. An extremely dry land surface stalls the westward motion of the storm. An extremely wet land surface, with greater surface roughness than the ocean, appears to weaken the storm with widespread weaker rainfall occurring. Improving the parameterization of ground wetness leads to a closer match between observed and predicted rainfall over both coastal and inland regions of the peninsula.

Further work is needed in all three areas of sensitivity addressed here. More cases need to be examined to see more clearly how the land surface processes affect land-fall and the subsequent behavior of tropical cyclones. It should be possible to increase the horizontal grid resolution further to a 20 km mesh. Finally, the issue of global versus regional modeling needs further experimentation.

Acknowledgements

We are indebted to Ms. Rosemarie Raymond, Ms. Terri Lapido and Ms. Sara Meador for technical assistance in the preparation of this work. The research reported here was supported equally by the following grants to the Florida State University: Navy Grant No. N00014–J–89–1476, NSF Grant No. ATM 8812053, and Grant No. INT 8713958. The computations were carried out on the National Center for Atmospheric Research Cray X–MP/48 computer. The authors acknowl-

edge the Supercomputer Computations Research Institute at Florida State University for facilities used in the production of graphics.

References

Anthes, R. A., Rosenthal, S. L. and Trout, J. W.: 1971, 'Preliminary Results from an Asymmetric Model of the Tropical Cyclone *Mon. Wea. Rev.* **99**, 744–758.

Blackadar, A. K.: 1979, 'High Resolution Models of the Planetary Boundary Layer', *Advances in Environmental Science and Engineering 1, No. 1*, Pfaffin and Ziegler (eds.), Gordon and Breach Sci. Pub., New York, pp. 50–85.

Carson, D. J. and Sangster, A. B.: 1981, *The Influence of Land-Surface Albedo and Soil Moisture on General Circulation Model Simulation*. Research Activities in Atmospheric and Oceanic Modelling (Ed. I. D. Rutherford). Numerical Experimentation Programme Report No. 2 pp. 5.14–5.21.

Chang, L. W.: 1978, 'Determination of Surface Flux of Sensible Heat, Latent Heat, and Momentum Utilizing the Bulk Richardson Number', *Pap. Meteorol. Res.*, **1**, 16–24.

Charnock, H.: 1955, 'Wind Stress on a Water Surface', *Quart. J. Roy. Meteorol. Soc.* **81**, 639–640.

Dickinson, R. E.: 1984, 'Modelling Evapotranspiration for Three Dimensional Global Climate Models', *Geophysical Monograph* **29**, A.G.U.

Haiyan He, McGinnis, J. W., Song, Z. and Yanai, M.: 1987, 'Onset of the Asian Summer Monsoon in 1979 and the Effect of the Tibetan Plateau', *Mon. Wea. Rev.* **115**, 1966–1995.

Hansen, J. and others: 1983, 'Efficient Three-Dimensional Global Models for Climate Studies: Models I and II, *Mon. Wea. Rev.* **111**, 609–662.

Kitoh, A., Yamazuki, K. and Tokioka, T.: 1988, 'Influence of Soil Moisture and Surface Albedo Changes over the African Tropical Rain Forest on Summer Climate Investigated with the MRI.GCM-I'. *J. Meteorol. Soc. Japan* **66**, 65–86.

Krishnamurti, T. N., Ardanuy, P. A., Ramanathan, Y. and Pasch, R.: 1981, 'On the Onset Vortex of the Summer Monsoon', *Mon. Wea. Rev.* **109**, 344–363.

Krishnamurti, T. N. and Subrahmanyam, D.: 1982, 'The 30–50 Day Mode at 850 mb during MONEX'. *J. Atmos. Sci.* **39**, 2088–2095.

Krishnamurti, T. N., Low-Nam, S. and Pasch, R.: 1983, 'Cumulus Parameterization and Rainfall Rates II', *Mon. Wea. Rev.* **111**, 815–828.

Krishnamurti, T. N. and Sheng, J.: 1985, 'The Heating Field in an Asymmetric Hurricane – Part I: Scale Analysis', *Adv. Atmos. Sci.* **2**, 402–413.

Krishnamurti, T. N.: 1985, 'Numerical Weather Prediction in Low Latitudes', *Advances in Geophysics* **28**, Academic Press.

Krishnamurti, T. N. and Sheng, J.: 1985, 'The Heating Field in an Asymmetric Hurricane – Part II: Results of Computations', *Adv. Atmos. Sci.* **2**, 426–445.

Krishnamurti, T. N., Bedi, H. S. and Oosterhof, D. K.: 1990, 'Precipitation Prediction over the Tropics from a Global Spectral Model'. *Atmosfera*, 1990 (in press).

Krishnamurti, T. N., Kumar, A., Yap, K. S., Dastoor, A. P., Davidson, N. and Sheng, J.: 1990, 'Prediction of Heavy Tropical Rainfall with a Meso-scale Model', *Advances in Geophysics* **32**, 133–286.

Manabe, S.: 1969a, 'Climate and the Ocean Circulation: I. The Atmospheric Circulation and the Hydrology of the Earth's Surface', *Mon. Wea. Rev.* **97**, 739–774.

Manobianco, J.: 1989, 'Explosive East Coast Cyclogenesis: Numerical Experimentation and Model Based Diagnostics'. *Mon. Wea. Rev.* **117**, 2384–2405.

Miller, B. I., Chase, P. P. and Jarvinen, B. R.: 1972, 'Numerical Prediction of Tropical Weather Systems', *Mon. Wea. Rev.* **100**, 825–835.

Mintz, Y.: 1984, *The Sensitivity of Numerically Simulated Climates to Land-Surface Boundary Conditions*, *The Global Climate*. J. T. Houghton (ed.), Cambridge University Press, pp. 79–105.

Romanova, E. N.: 1954, *The Influence of Forest Belts on the Vertical Structure of the Wind and on*

the Turbulent Exchange, Study of the Central Geophysical Observatory, No. 44 (106), Glavnaia Geofixicheskaia, Trudy, Leningrad, pp. 80–90.

Rowntree, P. R. and Bolton, J. A.: 1983, 'Simulation of the Atmospheric Response to Soil Moisture Anomalies over Europe'. *Quart. J. Roy. Metereol. Soc.* **190**, 501–526.

Sellers, P. J., Mintz, Y., Sud, Y. C. and Dalcher, A.: 1986, 'A Simple Biosphere Model (SiB) for use within General Circulation Models', *J. Atmos. Sci.* **43**, 505–531.

Sud, Y. C. and Fennessy, M.: 1984, 'Influence of Evaporation in Semi Arid Regions on the July Circulation: A Numerical Study', *J. Climatol.* **4**, 383–398.

Sud, Y. C. and Smith, W. E.: 1985, 'Influence of Local Land-Surface Processes on the Indian Monsoon: A Numerical Study', *J. Climate Appl. Meteorol.* **24**, 1015–1036.

Sud, Y. C. and Molod, A.: 1988, 'A GCM Simulation Study of the Influence of Sahara Evapotranspiration and Surface–Albedo Anomalies on July Circulation and Rainfall', *Mon. Wea. Rev.* **116**, 2388–2400.

Walker, J. and Rowntree, P. R.: 1977, 'The Effect of Soil Moisture on Circulation and Rainfall in a Tropical Model', *Quart. J. R. Meteorol. Soc.* **103**, 29–46.

Yamasaki, M.: 1975, 'A Numerical Experiment of the Interaction between Cumulus Convection and Large-Scale Motion', *Papers Meteor. Geophys.* **26**, 63–91.

Yamasaki, M.: 1986, 'A Three-Dimensional Tropical Cyclone Model with Parameterized Cumulus Convection', *Pap. Met. Geophys.* **37**, 205–334.

Yamasaki, M.: 1989, 'Numerical Experiments of Tropical Cyclones under Observed Situations with a New Scheme of Implicit Representation of Cumulus Convection', *18th Conference on Hurricanes and Tropical Meteorology*, May 16–19, San Diego, California, pp. 172–173.

Yanai, M., Esbensen, S. and Chu, J. H.: 1973, 'Determination of Bulk Properties of Tropical Cloud Clusters from Large Scale Heat and Moisture Budgets', *J. Atmos. Sci.* **30**, 611–627.

Yeh, T. C., Wetherrald, R. T. and Manabe, S.: 1984, 'The Effect of Soil Moisture on the Short-Term Climate and Hydrology Change. A Numerical Experiment', *Mon. Wea. Rev.* **112**, 474–490.